



Hierarchical functional layers on high-capacity lithium-excess cathodes for superior lithium ion batteries

Jianqing Zhao, Saad Aziz, Ying Wang*

Department of Mechanical and Industrial Engineering, Louisiana State University, Baton Rouge, LA 70803, United States

HIGHLIGHTS

- LMNCO nanoparticles were synthesized via using surfactant-assisted dispersion.
- The effect of ALD oxide coatings on LMNCO cathode has been systematically studied.
- Li-excess LMNCO core was modified with different Li-stoichiometric shell materials.
- Hierarch functional layers on LMNCO cathode contribute to improved rate capability.
- Surface-modified Li-excess cathode delivers high capacity of 259.8 mAh g⁻¹ at 1C.

GRAPHICAL ABSTRACT



ARTICLE INFO

Article history:

Received 7 June 2013

Received in revised form

15 August 2013

Accepted 17 August 2013

Available online 31 August 2013

Keywords:

Li-excess layered cathode material
Atomic layer deposition
Core–shell structure
Hierarchical functional layers
Lithium ion battery

ABSTRACT

Li-excess layered $\text{Li}[\text{Li}_{0.2}\text{Mn}_{0.54}\text{Ni}_{0.13}\text{Co}_{0.13}]_{\text{O}_2}$ (LMNCO) nanoparticles are facilely synthesized using a surfactant-assisted dispersion method. Ultrathin and conformal oxide coatings are deposited on the surface of individual LMNCO nanoparticle via atomic layer deposition (ALD). The effect of oxide ALD coatings on improving electrochemical performance of LMNCO electrodes is evaluated and optimized via tuning the coating thickness and composition. In addition, we synthesize a novel core–shell structure cathode consisting of Li-excess LMNCO as core and Li-stoichiometric material as shell, and its electrochemical property is optimized by tailoring weight content and composition of shell materials. Finally, electrochemical performance of Li-excess cathode material can be maximized by surface modification with hierach functional layers composed of 10 wt.% LiCoO_2 shell (~ 10 nm thick) and 6ZrO_2 ALD layers (~ 1 nm thick), which delivers very high initial discharge capacities of 296.4, 259.8, 156.6 and 104.2 mAh g⁻¹ at 0.1C, 1C, 5C and 10C, and can retain 184.0 mAh g⁻¹ at 1C after 100 electrochemical cycles. Such remarkably improved cycleability and rate capability of nanoarchitected Li-excess layered cathode material can be attributed to the synergic effect from hierarchical functional coatings to reduce electrochemical polarization, structural degradation and side reactions during electrochemical cycling.

© 2013 Elsevier B.V. All rights reserved.

1. Introduction

Rechargeable lithium ion battery has been demonstrated as an excellent electrochemical energy conservation and storage system. Tremendous research efforts have been focused on developing safe and environmentally friendly electrode materials that have high operating voltage, high energy density, excellent rate capability and

* Corresponding author. Tel.: +1 225 578 8577; fax: +1 225 578 9162.

E-mail address: ywang@lsu.edu (Y. Wang).



cycling stability [1,2]. The lithium alloys as anode materials for lithium ion batteries, such as lithium–silicon (Li–Si) and lithium–tin (Li–Sn), promise to provide excellent cycling stability, high rate capability, and higher specific capacity than conventional carbon materials with a theoretic capacity of 4000 and 990 mAh g⁻¹, respectively [3,4]. On the other hand, due to limited theoretical capacity and structural instability at high voltage, the traditional Li-stoichiometric cathode materials, e.g., layered LiCoO₂, spinel LiMn₂O₄, and olivine LiFePO₄, have low reversible specific capacity up to 170 mAh g⁻¹ [5]. The development of high-performance lithium ion batteries requires breakthrough increase in the capacity of cathode materials. Recently, Li-excess layered Li[Li_xM_{1-x}]O₂ (M = Mn, Ni, and Co) materials have attracted much research attention due to its high theoretical capacity (>250 mAh g⁻¹) and high operating potential (>4.5 V) [6–24]. The Li-excess oxide can be considered as either a solid solution or a composite oxide consisting of Li₂MnO₃ and LiMO₂ (M = Mn, Ni, and Co), in which LiMO₂ shares the same close-packing oxygen structure from a robust Mn-based layered structure of Li₂MnO₃ [5,7,22,23]. The structural compatibility between LiMO₂ and Li₂MnO₃ as layered rock-salt structures allows for their structural integration. The high capacity of Li-excess layered cathode material has been demonstrated from electrochemical activation of inert Li₂MnO₃ at the initial charge to 4.8 V vs. Li/Li⁺. In this electrochemical activation process oxygen will be irreversibly lost together with lithium ion extraction as lithia when Li₂MnO₃ is decomposed to Li₂O and MnO₂. Hence, the oxidation state of the transition metal ions is decreased in comparison with that in the initial material at the end of the first discharge to 2.0 V vs. Li/Li⁺ [6,13,25]. The initial Li₂MnO₃ activation contributes to the high capacity of Li-excess layered cathode in the subsequent electrochemical cycles but also the low Coulombic efficiency of the first cycle. However, the easy oxidation in transition metal redox pairs during the initial Li₂MnO₃ activation induces severe decomposition of electrolyte [29]. Subsequently, phase transformation and transition metal dissolution occur in the layered structure of Li-excess cathode due to the elimination of oxygen ion vacancies via atomic rearrangements, resulting in significant irreversible capacity loss and structural instability of working electrode [17]. In spite of the high capacity, these layered cathode materials suffer from significant irreversible capacity loss in the initial charge/discharge, inferior rate capability and poor reversibility. The unfavorable cycling performance of Li-excess layered cathode materials at high charge/discharge rates can be attributed to structural rearrangement, poor electronic conductivity and severe side reactions on the cathode surface [6,7,15,19,24,25]. These factors summarized above together hinder the commercial application of Li-excess layered cathode materials.

Several approaches have been reported to solve the issues of Li-excess layered cathode materials mentioned above via metal ion doping, surface modification, preparing nanocomposite, and fabricating nano-sized materials [14,26–36]. Surface modification is extensively utilized due to its simplicity and effectiveness. A variety of surface coatings have been synthesized to ameliorate properties of underlying Li-excess cathodes, and thus improve its reversibility, rate capability and cycleability [5,37]. The coating materials can be divided into two categories: Li-active and Li-inert materials. To date, Li-inert coating materials reported in literature include metal oxides [25,28], metal fluorides [26,27], metal phosphates [26,29], carbon-based materials [24,36], and so on. Among these inert coating materials, surface modification via oxide coatings (e.g., Al₂O₃, ZnO, ZrO₂, MgO, MnO, SnO₂ and CeO₂) has been demonstrated as one of the most effective approaches to improve cycling performance of Li-excess layered cathodes [12,26,28,33]. The oxide coating not only serve as a physical protection barrier that prevents cathode from direct contact with non-aqueous

electrolyte but also as a HF scavenger that reduces acidity of electrolyte. In addition, the oxide film can act as a solid framework to restrict the disordered phase transformation, leading to better structural stability [25,38,39]. However, surface modifications with electrochemically inactive materials will decrease the energy and volumetric densities of active cathode materials and affect lithium ion and electron transfer in working electrodes [40]. Compared to thick and incomplete oxide coatings prepared by traditional wet chemical methods, films grown using atomic layer deposition (ALD) are uniform, dense, homogenous, pinhole-free, and extremely conformal to the underlying substrate, and the thickness of coatings can be precisely controlled at atomic level [41–46]. ALD is a thin film deposition subjected to a sequence of chemisorption and self-terminating surface reactions. ALD oxide coatings have been used to enhance electrochemical performance of common cathode materials, such as LiCoO₂ [41,42] and LiMn₂O₄ [43,46]. However, there are only a few reports investigating the effect of oxide ALD coatings on Li-excess layered cathode materials [25].

On the other hand, fabrication of core–shell structures via “wet-chemical” methods is a common route to introduce Li-active materials as shells on the surface of core materials [14,21,40,47–52]. The electrochemically-active shells can improve electronic conductivity, lithium ion diffusivity, thermal stability, and cycling stability of core Li-excess cathode materials. In order to improve cycling stability, X. Yang et al. employed Li-rich Li_{1.15}[Ni_{1/4}Mn_{3/4}]_{0.85}O₂ as the shell enwrapping core Li_{1.15}[Ni_{1/3}Co_{1/3}Mn_{1/3}]_{0.85}O₂. The as-prepared core–shell composite shows significantly enhanced cycling performance, due to better structural stability of the core–shell structure [51]. D. Kim et al. introduced spinel Li-poor Li_{0.5}Mn_{0.65}Ni_{0.35}O₂ shell on core 0.3Li₂MnO₃·0.7LiMn_{0.5}Ni_{0.5}O₂ cathode, which can decrease lithium content in the parent ‘layered–layered’ structure and enhance its electrochemical property [14]. Q. Qiao et al. have reported that coating LiMnPO₄ on the surface of Li-rich layered Li[Li_{0.17}Ni_{0.25}Mn_{0.58}]O₂ followed by heat treatment can increase reaction kinetics and structural stability of core material, resulting in better rate capability and cycleability in comparison with bare cathode [52]. Overall, core–shell structured composites have been designed to combine advantages from both core and shell materials for enhanced electrochemical performance.

Among solid solutions of layered cathode materials, Li[Li_{0.2}Mn_{0.54}Ni_{0.13}Co_{0.13}]O₂ in a two component notation as 0.5Li₂MnO₃·0.5LiMn_{1/3}Ni_{1/3}Co_{1/3}O₂ (hereafter marked as LMNCO) has received particular interest, due to its higher theoretical capacity of 321 mAh g⁻¹, better cycling stability and rate capability than other Li-rich analogs; thus it is an excellent candidate as cathode for applications in superior lithium ion batteries with high energy and high power [53,54]. As shown in Fig. 1, hierarchical functional layers on LMNCO cathode are designed in this work and expected to achieve a synergistic effect from ALD oxide coating and core–shell structure for superior battery performance. We first synthesize Li[Li_{0.2}Mn_{0.54}Ni_{0.13}Co_{0.13}]O₂ nanoparticles by using surfactant-assisted dispersion. The triblock co-polymer F127 serves as the dispersant in sol–gel method. In comparison with micro-sized materials, nanomaterials offer more active sites for lithium ion insertion and extraction due to the larger surface-to-volume ratio, and provide more flexibility for volume expansion/contraction during lithiation/delithiation process, resulting in higher specific capacity and improved cycleability. Furthermore, nanomaterials provide larger electrode/electrolyte contact area and shorter lithium ion diffusion path, leading to superior rate capability. However, associated with these benefits, the high surface area and complex structure of nanomaterials will exacerbate undesirable side reactions in terms of decomposition of electrolyte and dissolution of transition metal ions [37]. In order to improve



Fig. 1. Schematic diagram showing preparation and surface modifications of $\text{Li}[\text{Li}_{0.2}\text{Mn}_{0.54}\text{Ni}_{0.13}\text{Co}_{0.13}]O_2$ nanoparticles.

cycleability and rate capability of Li-excess layered LMNCO nanomaterials, we systematically evaluate the effects of ALD oxide coatings on LMNCO nanoparticles (marked as $n\text{M}_x\text{O}_y$ ALD@LMNCO, $M = \text{Zn, Zr, and Al}$, n is the ALD coating layers) via tuning ALD coating thickness and composition. In addition, we synthesize core–shell-structured composite cathode consisting of Li-stoichiometric materials (LiM_xO_y , $M = \text{Mn and Co}$) as shell and Li-excess LMNCO as core material (marked as $\text{LM}_x\text{O}_y\text{-X@LMNCO}$, $M = \text{Mn and Co}$, X is the weight content of shell materials) and optimize the performance of core–shell cathode by tailoring weight content of shell and changing composition of shell materials. Finally, electrochemical performance of LMNCO cathode can be maximized by depositing hierarchical functional layers on LMNCO nanoparticles consisting of 10 wt.% LiCoO_2 as a shell followed by coating 6 ZrO_2 ALD layers (marked as 6 ZrO_2 ALD@LCO-10@LMNCO). The 6 ZrO_2 ALD@LCO-10@LMNCO composite shows superior cycling stability and rate capability due to the synergic and cooperative effects from LiCoO_2 shell (~ 10 nm thickness) and ultrathin ZrO_2 coating (~ 1 nm thickness) that improve the electronic conductivity of cathode and reduce side reactions during electrochemical cycling.

2. Experimental

2.1. Synthesis of Li-excess $\text{Li}[\text{Li}_{0.2}\text{Mn}_{0.54}\text{Ni}_{0.13}\text{Co}_{0.13}]O_2$ nanoparticles

The Li-excess $\text{Li}[\text{Li}_{0.2}\text{Mn}_{0.54}\text{Ni}_{0.13}\text{Co}_{0.13}]O_2$ nanoparticles were synthesized by using surfactant-assisted dispersion. We first prepared three precursor solutions: 0.54 mmol F127 ($\text{EO}_{106}\text{PO}_{70}\text{EO}_{106}$) as the dispersant in 50 ml ethanol, 0.08 mol transition metal acetates (a molar ratio of $\text{Mn}^{2+}:\text{Ni}^{2+}:\text{Co}^{2+} = 0.54:0.13:0.13$) in 50 ml ethanol, and 0.12 mol lithium hydroxide in 20 ml distilled water. The molar ratio of F127/ Mn^{2+} was set to 0.01. The transition metal precursor solution was dropwisely dropped into F127/ethanol solution under continuous stirring at 40 °C, and then the lithium precursor solution was added. The mixed solution was heated at 80 °C until the solvent was completely evaporated. Afterward, the mixture was dried in air at 120 °C for 12 h. The heat treatment of dried mixture was carried out in air at 300 °C for 3 h, followed by sintering at 900 °C for 12 h and quenching in distilled water. The $\text{Li}[\text{Li}_{0.2}\text{Mn}_{0.54}\text{Ni}_{0.13}\text{Co}_{0.13}]O_2$ nanoparticles were collected after being completely dried in vacuum overnight.

2.2. Atomic layer deposition of different oxide coatings on $\text{Li}[\text{Li}_{0.2}\text{Mn}_{0.54}\text{Ni}_{0.13}\text{Co}_{0.13}]O_2$ nanoparticles

Atomic layer deposition of different oxide coatings on LMNCO nanoparticles was performed in a Savannah 100 ALD system (Cambridge NanoTech Inc.) at 120 °C. ZnO ALD coating was carried out using $\text{Zn}(\text{CH}_2\text{CH}_3)_2$ (diethylzinc, DEZ) and H_2O as precursors

with exposure time of 0.03 and 0.03 s, waiting time of 10 and 10 s, purge time of 40 and 40 s, respectively. ZrO_2 ALD coating was obtained by using $\text{Zr}(\text{OC}(\text{CH}_3)_3)_4$ (Zirconium *tert*-butoxide, ZTB) and H_2O as precursors with exposure time of 0.03 and 0.5 s, waiting time of 10 and 10 s and purge time of 40 s and 60 s, respectively. Al_2O_3 ALD coating was achieved applying $\text{Al}(\text{CH}_3)_3$ (Trimethylaluminum, TMA) and H_2O as precursors with exposure time of 0.02 and 0.02 s, waiting time of 10 and 10 s and purge time of 40 s and 40 s, respectively. The principle of oxide ALD growth from H_2O and metallic precursors is subjected to the two self-terminating reactions, which can be referred from our previous works [38,39,46].

2.3. Preparation of $\text{LiCoO}_2@\text{Li}[\text{Li}_{0.2}\text{Mn}_{0.54}\text{Ni}_{0.13}\text{Co}_{0.13}]O_2$ core–shell structure

Stoichiometric molar ratio of lithium acetate and cobalt acetate were first dissolved in distilled water. $\text{Li}[\text{Li}_{0.2}\text{Mn}_{0.54}\text{Ni}_{0.13}\text{Co}_{0.13}]O_2$ powders were dispersed in the above solution. The mixed solution was sonicated for 30 min, and then stirred at 80 °C to evaporate the distilled water. After being dried in air overnight at 120 °C, the mixture composed of LMNCO powders and Li and Co precursor was sintered in air at 750 °C for 12 h. The weight ratio of core $\text{Li}[\text{Li}_{0.2}\text{Mn}_{0.54}\text{Ni}_{0.13}\text{Co}_{0.13}]O_2$ and shell LiCoO_2 can be controlled via tuning the mass of $\text{Li}[\text{Li}_{0.2}\text{Mn}_{0.54}\text{Ni}_{0.13}\text{Co}_{0.13}]O_2$ powders and Li and Co precursors. The same procedure was used to prepare LiMn_2O_4 and LiCoMnO_4 as shell materials on core $\text{Li}[\text{Li}_{0.2}\text{Mn}_{0.54}\text{Ni}_{0.13}\text{Co}_{0.13}]O_2$ by using corresponding transition metal precursors.

2.4. Hierarchical functional layers coating on core $\text{Li}[\text{Li}_{0.2}\text{Mn}_{0.54}\text{Ni}_{0.13}\text{Co}_{0.13}]O_2$ nanoparticles

To deposit hierarchical functional layers on core $\text{Li}[\text{Li}_{0.2}\text{Mn}_{0.54}\text{Ni}_{0.13}\text{Co}_{0.13}]O_2$ nanoparticles, the as-prepared core–shell structure was coated with ALD oxide film. The $\text{Li}[\text{Li}_{0.2}\text{Mn}_{0.54}\text{Ni}_{0.13}\text{Co}_{0.13}]O_2$ nanoparticles was modified with 10 wt.% LiCoO_2 shell, followed by coating of 6 ZrO_2 ALD layers.

2.5. Characterizations

The crystallographic structure of $\text{Li}[\text{Li}_{0.2}\text{Mn}_{0.54}\text{Ni}_{0.13}\text{Co}_{0.13}]O_2$ nanoparticles was examined by X-ray diffraction (XRD) using a Rigaku MiniFlex X-ray diffractometer with Cu K_α radiation at a scan rate of 2°min^{-1} . Morphology and particle size of LMNCO nanoparticles were observed using a FEI Quanta 3D FEG field emission scanning electron microscopy (FESEM). Transmission electron microscopy (TEM) images were captured on a JEM-2010 instrument microscope at an acceleration voltage of 200 kV, to examine morphology and structure of bare and surface modified LMNCO nanoparticles.

2.6. Electrochemical measurements

The working electrodes were composed of 75 wt.% bare or surface modified Li[Li_{0.2}Mn_{0.54}Ni_{0.13}Co_{0.13}]O₂ nanoparticles, 20 wt.% acetylene black (conductive carbon, Alfa Aesar, 99.5%), and 5 wt.% poly-vinylidenefluoride (PVDF, Alfa Aesar) as the binder. These cathodes were assembled into two-electrode CR2032-type coin cells for electrochemical measurements, with metallic lithium foil as anode, Celgard-2320 membrane as separator; electrolyte was 1 M LiPF₆ dissolved in ethylene carbonate (EC) and dimethyl carbonate (DMC) and diethyl carbonate (DEC) at a volumetric ratio of 1:1:1. Galvanostatic charge and discharge were performed at different current densities in a voltage range of 2.0–4.8 V using an 8-channel battery analyzer (MTI Corporation). Theoretical capacities of bare and surface modified Li[Li_{0.2}Mn_{0.54}Ni_{0.13}Co_{0.13}]O₂ cathode materials are all set to 250 mAh g⁻¹, i.e., current density corresponding to 1C is 250 mA g⁻¹. Electrochemical storage capacities of working electrodes were calculated based on the mass of active cathode materials. Cyclic voltammetric (CV) curves of different cathodes were recorded at a scanning rate of 0.1 mV s⁻¹ between 2.0 and 4.8 V using an electrochemical analyzer (CHI 605C).

3. Results and discussion

The pristine Li[Li_{0.2}Mn_{0.54}Ni_{0.13}Co_{0.13}]O₂ can be considered as a solid solution composite, composed of Li-inactive Li₂MnO₃ and Li-active LiMn_{1/3}Ni_{1/3}Co_{1/3}O₂ two phases with a molar ratio of 1:1 in an integrated layered structure [9,29]. XRD pattern in Fig. 2a illustrates the predominant layered structure of LMNCO with group space R-3m. The weak diffraction peak located around $2\theta = 20\text{--}25^\circ$ indicates the super lattice structure, which is resulted from the LiMn₆ cation arrangement in the transition metal layers of Li₂MnO₃ component (group space C2m) [10,18,22]. The Li-excess layered LMNCO nanoparticles with an average particle size of ~250 nm have been facilely prepared via using surfactant dispersion, as shown in SEM image (Fig. 2b) and TEM image (Fig. 3a).

3.1. Improving and optimizing electrochemical performance of LMNCO via oxide ALD coatings

In this section, the optimal thickness for maximizing cycling performance is determined via tailoring ZnO ALD coatings on LMNCO nanoparticles, and effects of various ALD oxide coatings on improving electrochemical properties of LMNCO cathode are compared for the first time. TEM images in Fig. 3b and c show ZnO

and ZrO₂ ALD coatings that are conformal, homogeneous, uniform and crystalline. 50 ALD growth cycles contribute to the thickness of 9.7 nm for ZnO and 6.5 nm for ZrO₂ on the surface of LMNCO nanoparticles, corresponding to the ALD growth rate of 1.94 Å/cycle for ZnO, 1.30 Å/cycle for ZrO₂, respectively.

Fig. 4 summarizes the effects of ultrathin oxide ALD coatings on LMNCO nanoparticles on improving electrochemical performance via tuning ALD coating thickness and composition. Thus, we compare cycling performances of LMNCO nanoparticles coated with two, six, and ten ZnO ALD layers, and those of LMNCO modified with ZnO, ZrO₂ and Al₂O₃ ALD coatings. As shown in Fig. 4a, bare LMNCO suffers from drastic capacity fading from the initial discharge capacity of 114.5 mAh g⁻¹ to 65.9 mAh g⁻¹ after 100 electrochemical cycles at 1C (250 mA g⁻¹). On the contrary, LMNCO coated with ZnO ALD film exhibits improved capacity retentions in comparison with bare cathode. The enhanced electrochemical performance can be attributed to the protective ZnO ALD coating that reduces decomposition of electrolyte and preserves structural stability of LMNCO cathode. 6ZnO ALD layers demonstrate to have optimal thickness (1.14 nm via 6ALD growth layers) for the best performance of LMNCO nanoparticles, consistent with the optimal Al₂O₃ ALD coatings on the surface of LMNCO via 6 ALD growth cycles in the reported work [25]. We speculate that two ZnO ALD layers (0.388 nm thick) are too thin to provide sufficient mechanical protection and to consume the HF in electrolyte, while thicker ZnO coating composed of ten ZnO ALD layers (1.94 nm thick) may slow down the lithium ion diffusion at a high current density of 250 mAh g⁻¹ [38].

Fig. 4b–d compares initial charge/discharge capacities and rate performances of bare LMNCO and LMNCO nanoparticles coated with 6ZnO, 6ZrO₂ and 6Al₂O₃ ALD layers. It can be seen that all ALD modified LMNCO cathodes show improved cycleability, Coulombic efficiencies in the initial cycle and rate capability than bare cathode. In particular, 6ZrO₂ ALD layers demonstrate as the most effective coating, followed by ZnO and Al₂O₃, on improving performance of LMNCO especially at high charge/discharge rates as shown in Fig. 4d. Bare LMNCO delivers an initial charge capacity of 397.1 mAh g⁻¹ and discharge capacity of 228.4 mAh g⁻¹ at 0.1C (Fig. 4c), corresponding to a very low Coulombic efficiency of 58.3%. The high irreversible capacity loss of pristine LMNCO can be ascribed to intense decomposition of organic electrolyte on the large surface of LMNCO nanoparticles together with structural disorder of LMNCO caused by transition metal dissolutions in LMO₂ (M = Mn, Ni and Co) and irreversible oxygen loss in Li₂MnO₃ component. In contrast, LMNCO coated with 6ZrO₂ ALD layers (~1 nm thick) exhibit a much higher Coulombic efficiency of 83.3%

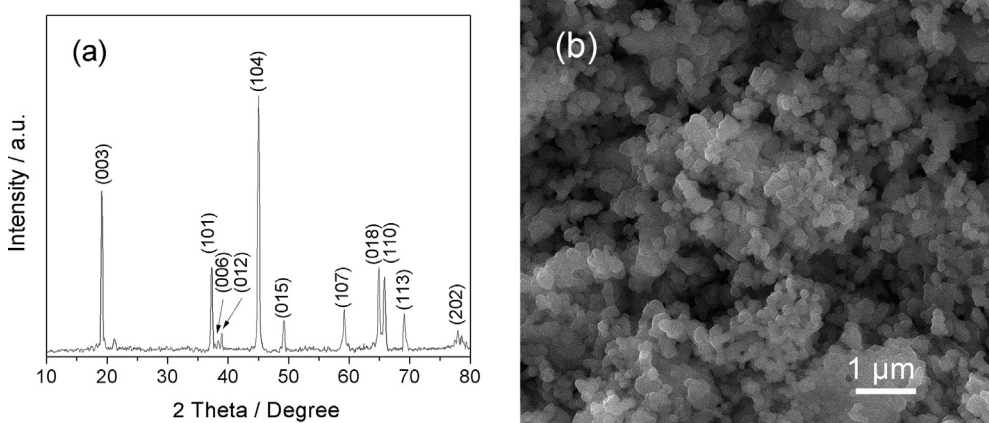


Fig. 2. (a) XRD pattern and (b) scanning electron microscopic (SEM) image of Li[Li_{0.2}Mn_{0.54}Ni_{0.13}Co_{0.13}]O₂ powders.

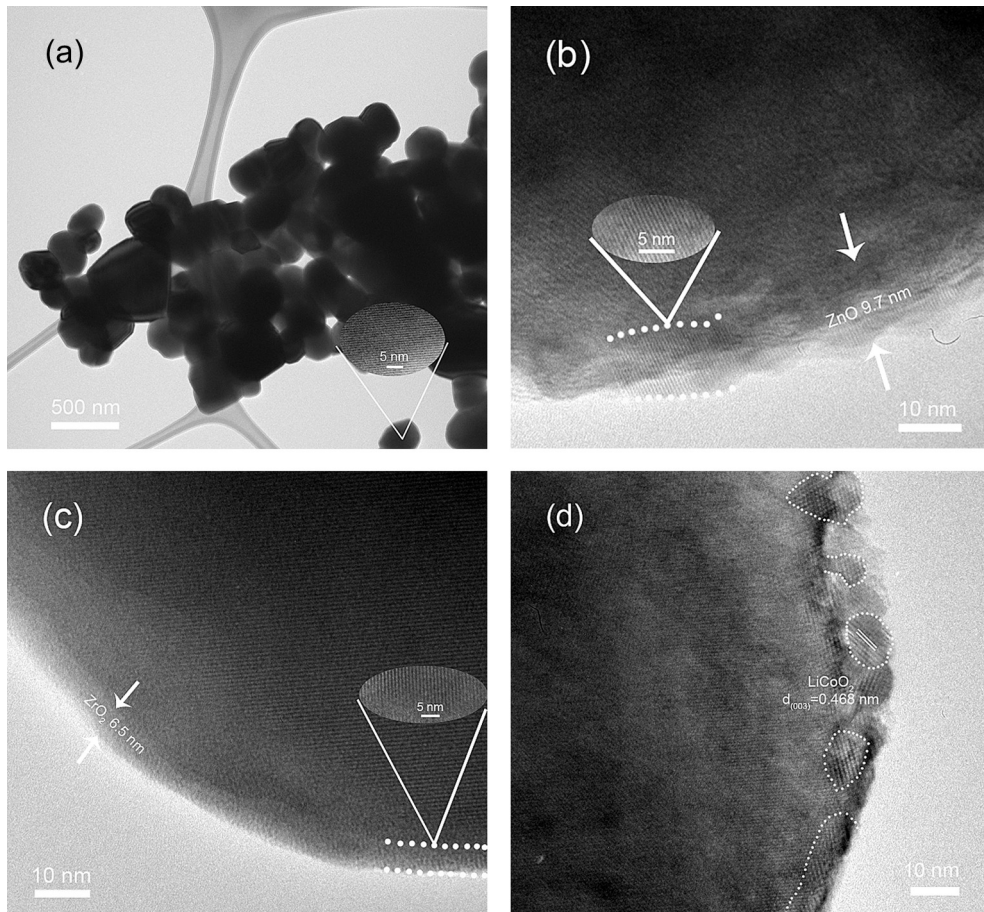


Fig. 3. Transmission electron microscopic (TEM) images with inserted high-resolution lattice fringes of (a) bare $\text{Li}[\text{Li}_{0.2}\text{Mn}_{0.54}\text{Ni}_{0.13}\text{Co}_{0.13}]_{\text{O}_2}$ nanoparticles, and $\text{Li}[\text{Li}_{0.2}\text{Mn}_{0.54}\text{Ni}_{0.13}\text{Co}_{0.13}]_{\text{O}_2}$ particle coated with (b) 50ZnO ALD layers, (c) 50ZrO₂ ALD layers and (d) 10 wt.% LiCoO₂ shell.

and specific discharge capacity of 274.9 mAh g⁻¹, due to the conformal and complete coverage of ALD film on individual LMNCO nanoparticle. The 6ZrO₂ ALD@LMNCO also shows improved cycling stability in comparison with that of bare LMNCO by retaining a discharge capacity of 123.0 mAh g⁻¹ after 100 cycles at 1C and delivering a capacity retention of 80.4%, while bare LMNCO nanoparticles exhibit a final capacity of 65.9 mAh g⁻¹ and a capacity retention of only 65.6% (Fig. 4b). Compared to ZnO and Al₂O₃ coated LMNCO cathodes, better high-rate cycling performance of 6ZrO₂ ALD@LMNCO in Fig. 3d may be attributed to the formation of lithium ion conductive interphase, Li–Zr–O or Li–M–Zr–O (M = Mn, Ni and Co), between LMNCO bulk and ZrO₂ coating [25,46]. However, ZrO₂ ALD coating for enhancing rate capability of LMNCO cathode is limited by the inferior conductivity of LMNCO nanoparticles and semi-conductivity of ZrO₂ coating. As for Al₂O₃ ALD coating, although Al₂O₃ ALD coating has been demonstrated to improve electrochemical performance of LMNCO cathodes at low current densities less than 1C (Fig. 4c), which has also been reported in others' [25], the electronically insulating Al₂O₃ coating affects high-rate capacities of Al₂O₃ ALD modified LMNCO cathodes when the current density is higher than 2C, as shown in Fig. 4d.

Cyclic voltammetric (CV) performances are then carried out to understand the effect of ZrO₂ ALD coating on electrochemical performance of LMNCO cathode, as presented in Fig. 4e and f. The peaks in CV curves correspond to oxidation and reduction of transition metal redox pairs that occur upon lithium ion extraction and insertion in LMNCO layered structure. Fig. 4e reveals the first three cycles of CV measurement of bare LMNCO cathode. The first

anodic peak at 4.16 V in the initial charge curve is associated with the oxidation of Ni^{2+} to Ni^{4+} followed by Co^{3+} to Co^{4+} , whereas Mn still remains as tetravalent in $\text{LiMn}_{1/3}\text{Ni}_{1/3}\text{Co}_{1/3}\text{O}_2$ structure [31,55]. The second anodic peak at 4.65 V corresponds to the decomposition of Li_2MnO_3 to Li_2O and MnO_2 , along with the unavoidable decomposition of electrolyte and the formation of solid electrolyte interphase (SEI) at such high potential >4.5 V [35]. Such electrochemical activation process of Li_2MnO_3 would result in the low Coulombic efficiency in the first cycle and high capacity of Li-excess layered cathode materials via simultaneously losing oxygen irreversibly as Li_2O and yielding Li-active MnO_2 component. In the initial discharge curve of the same sample, reduction of Co^{4+} to Co^{3+} and Ni^{4+} to Ni^{2+} occurs at 3.63 V, and the cathodic peak at 3.26 V can be assigned to the reduction of Mn^{4+} to Mn^{3+} from the as-activated MnO_2 component [35]. The anodic and cathodic peaks in the first CV cycle are consistent with the voltage plateaus in the first charge/discharge profiles of LMNCO in Fig. 4c. It can be seen from the second and third CV cycles in Fig. 4e that the peak observed at 4.65 V in the initial CV curve disappears leaving only one anodic peak at 4.16 V. The corresponding cathodic peak associated with reduction of $\text{Ni}^{2+}/\text{Ni}^{4+}$ and $\text{Co}^{3+}/\text{Co}^{4+}$ redox pairs shifts obviously towards the higher voltage region at 3.75 V, and the cathodic peak related to reduction of $\text{Mn}^{3+}/\text{Mn}^{4+}$ redox at 3.26 V becomes more distinct, indicating better reversibility of transition metal redox pairs in bare LMNCO cathode after the initial activation process. In the case of the CV curves of LMNCO coated with 6ZrO₂ ALD layers (~1 nm thick) as shown in Fig. 4f, the anodic peak in the first CV cycle related to oxidation of $\text{Ni}^{2+}/\text{Ni}^{4+}$ and $\text{Co}^{3+}/\text{Co}^{4+}$ redox

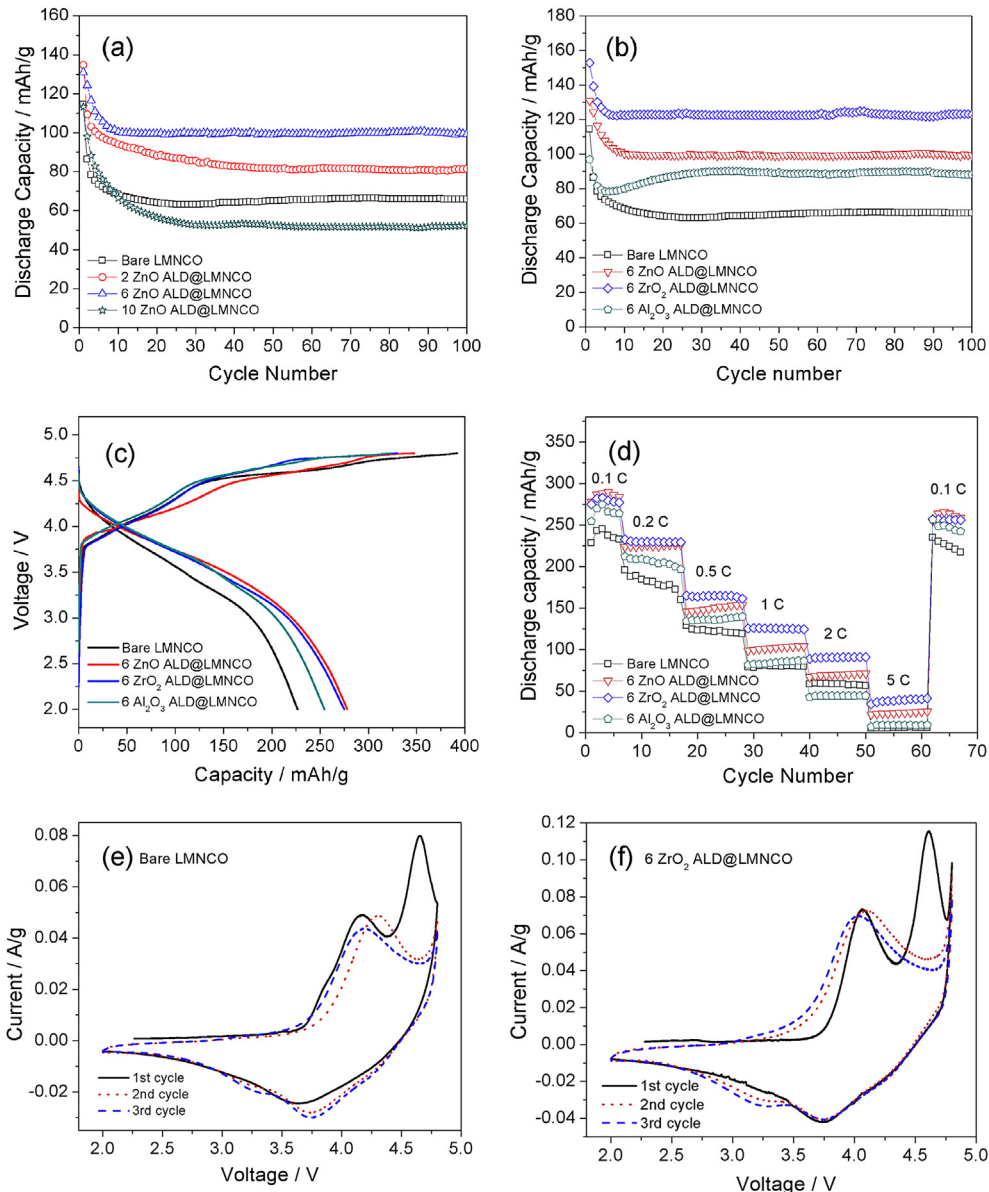


Fig. 4. Electrochemical performances of different ALD-modified $\text{Li}[\text{Li}_{0.2}\text{Mn}_{0.54}\text{Ni}_{0.13}\text{Co}_{0.13}] \text{O}_2$ nanoparticles coated with 2, 6 and 10ZnO ALD layers in comparison with bare electrode at a current density of 250 mA g^{-1} (1C); (b) cycling performances at a current density of 250 mA g^{-1} (1C) and (c) the initial charge and discharge curves at a current density of 25 mA g^{-1} (0.1C) and (d) rate performances at different current densities of $\text{Li}[\text{Li}_{0.2}\text{Mn}_{0.54}\text{Ni}_{0.13}\text{Co}_{0.13}] \text{O}_2$ nanoparticles coated with 6ZnO, 6 ZrO_2 and 6 Al_2O_3 ALD layers in comparison with bare electrode; the first three CV profiles of (e) bare electrode and (f) $\text{Li}[\text{Li}_{0.2}\text{Mn}_{0.54}\text{Ni}_{0.13}\text{Co}_{0.13}] \text{O}_2$ nanoparticles coated with 6 ZrO_2 ALD layers at a scanning rate of 0.1 mV s^{-1} “Bare LMNCO”: bare $\text{Li}[\text{Li}_{0.2}\text{Mn}_{0.54}\text{Ni}_{0.13}\text{Co}_{0.13}] \text{O}_2$ nanoparticles; “ $n\text{M}_x\text{O}_y$ ALD@LMNCO ($M = \text{Zn}, \text{Zr}$ and Al)”: $\text{Li}[\text{Li}_{0.2}\text{Mn}_{0.54}\text{Ni}_{0.13}\text{Co}_{0.13}] \text{O}_2$ nanoparticles coated with $n\text{M}_x\text{O}_y$ ALD layers.

pairs is sharper with even higher current in comparison with that of pristine LMNCO. It can also be found that the subsequent initial activation peak separates two sharp anodic peaks at 4.60 V and around 4.8 V. The former peak is attributed to the activation of Li_2MnO_3 and the latter can probably be ascribed to decomposition of electrolyte and formation of SEI film on the surface of electrode. Such intriguing electrochemical phenomenon indicates that ZrO_2 coating can effectively reduce decomposition of electrolyte during the activation procedure of Li_2MnO_3 , and thus facilitates complete activation of Li_2MnO_3 , leading to less electrochemical polarization, higher specific capacity and better structural stability of LMNCO cathode. However, decomposition of electrolyte cannot be avoided due to the high oxidation abilities of $\text{Mn}^{3+}/\text{Mn}^{4+}$, $\text{Ni}^{2+}/\text{Ni}^{4+}$ and $\text{Co}^{3+}/\text{Co}^{4+}$ redox pairs. The corresponding reduction of $\text{Ni}^{2+}/\text{Ni}^{4+}$

and $\text{Co}^{3+}/\text{Co}^{4+}$ redox pairs at 3.75 V is more reversible, resulting in smaller overpotential of 0.32 V than 0.53 V of bare LMNCO (Fig. 4e). The cathodic peak at 3.20 V becomes sharper in the second and third CV cycles, indicating easier reduction of $\text{Mn}^{3+}/\text{Mn}^{4+}$ redox in later cycles. Furthermore, CV profiles of 6 ZrO_2 ALD@LMNCO in the second and third cycles are almost identical to each other, though both lose the irreversible activation peak from the CV curve of the first cycle, demonstrating the remarkable improved reversibility of 6 ZrO_2 ALD@LMNCO in comparison with bare LMNCO.

Overall, electrochemical performances of various electrodes in Fig. 4 illustrate that surface modifications of Li-excess layered cathode material – $\text{Li}[\text{Li}_{0.2}\text{Mn}_{0.54}\text{Ni}_{0.13}\text{Co}_{0.13}] \text{O}_2$ and tailoring oxide ALD coatings can effectively reduce decomposition of electrolyte in the initial activation process of Li_2MnO_3 and alleviate structural

degradation in subsequent cycles. The ALD-modified LMNCO cathodes show increased Coulombic efficiency in the initial cycle, higher specific capacity and enhanced cyclability in comparison with bare LMNCO electrode. The optimal thickness of ALD oxide coating for LMNCO nanoparticles is ~1 nm composed of 6 oxide ALD layers. ZrO_2 is the most effective oxide coating to improve performance of LMNCO electrodes, followed by ZnO and Al_2O_3 . However, ZrO_2 ALD coating does not show significant effect in improving rate capability of LMNCO coated due to poor electronic conductivity of ZrO_2 coatings as shown in Fig. 4d. Hence, an alternative surface modification approach is used to improve high-rate performance of Li-excess layered cathode materials.

3.2. Improving and optimizing electrochemical performance of LMNCO via fabricating core–shell structures

The low electronic conductivity and lithium ion diffusivity of Li-excess layered $Li[Li_{0.2}Mn_{0.54}Ni_{0.13}Co_{0.13}]O_2$ cathode material impedes the improvement of high rate capability. The effort of reducing the particle size of LMNCO to nano-sized particles has been achieved in Figs. 2b and 3a in order to decrease the pathway of lithium ion diffusion for enhanced rate capability of LMNCO cathode. However, the electrochemical performance in Fig. 4 shows inferior high-rate cycling performance of pristine LMNCO nanoparticles when charged at high current densities larger than 1C. Although ultrathin and conformal ZrO_2 ALD coating with the optimal thickness of ~1 nm has been demonstrated to enhance the electrochemical performance of LMNCO nanoparticles, the electrochemically inert ZrO_2 is unfavorable for facilitating both lithium

ion diffusion and interfacial charge transfer of the electrode. One solution is to introduce more conductive Li-active phase on the surface of LMNCO nanoparticles for improved rate capacities of LMNCO. Herein, we deposit Li-stoichiometric layered $LiCoO_2$, spinel $LiMn_2O_4$ and layered-spinel $LiCoMnO_4$ as shells on LMNCO core to improve rate capability of LMNCO cathode. The three shell materials all have better electronic conductivity and lithium ion diffusivity than that of LMNCO core [56]. Electrochemical performance of such nanoarchitected composites are evaluated and optimized at 1C, by varying the composition and weight content of shell materials.

Fig. 5a and b summarizes cycling performances of $LM_xO_y-X@LMNCO$ electrodes with different weight fraction and composition of shell materials. It can be seen that $LiCoO_2$ as shell in a series of 5 wt.%, 10 wt.%, 25 wt.%, and 50 wt.% can all effectively improve specific capacities in comparison with bare LMNCO nanoparticles, while 10 wt.% of $LiCoO_2$ shell is the optimal weight percentage and shows the most significant effect in improving performance of LMNCO. Fig. 3d presents HRTEM image of LCO-10@LMNCO displaying the core–shell structure, with crystalline $LiCoO_2$ nanoparticles on the surface of LMNCO particle forming a ~10 nm thick coverage. Composition of $LiCoO_2$ is confirmed by lattice fringes in the HRTEM image. The core–shell LCO-10@LMNCO delivers better performance than bare LMNCO, due to better electronic conductivity and higher Li-ion diffusivity of $LiCoO_2$. For example, LCO-10@LMNCO delivers a high initial discharge capacity of 187.5 mAh g⁻¹ and retains 132.8 mAh g⁻¹ after 100 electrochemical cycles, much higher than the initial discharge capacity of 114.5 mAh g⁻¹ and final capacity of 65.9 mAh g⁻¹ at 100th cycle

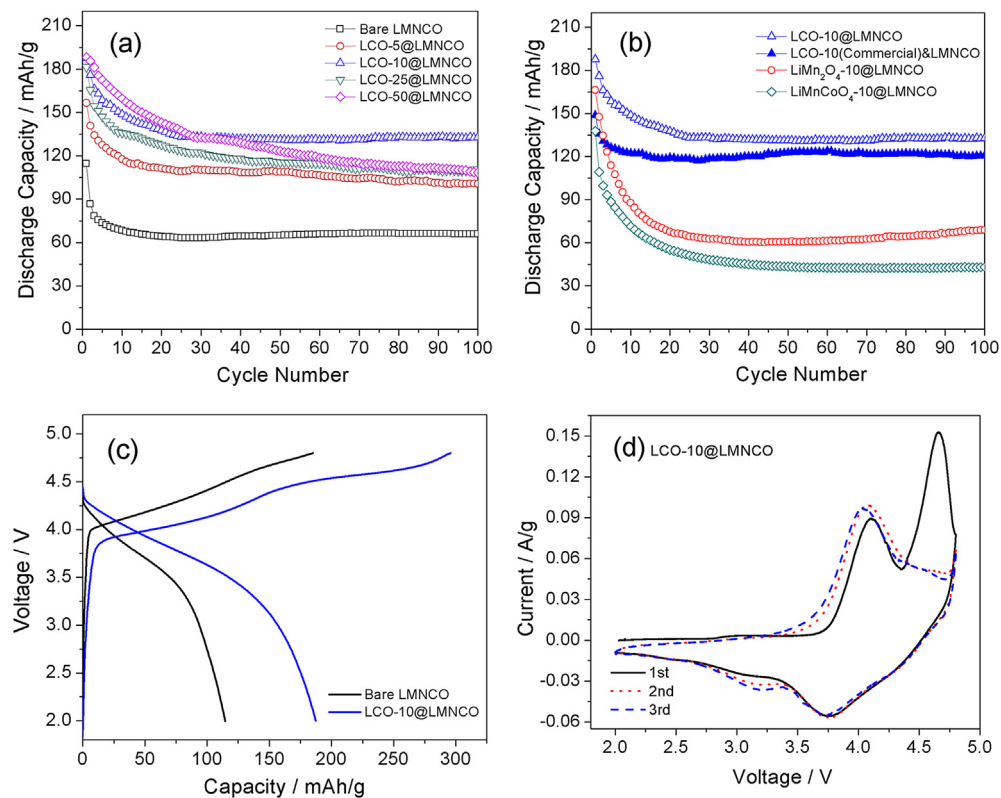


Fig. 5. Electrochemical performances of different core–shell-structured $Li[Li_{0.2}Mn_{0.54}Ni_{0.13}Co_{0.13}]O_2$ nanoparticles modified with (a) $LiCoO_2$ shell of 5 wt.%, 10 wt.%, 25 wt.%, and 50 wt.% in comparison with bare electrode and (b) different shells ($LiCoO_2$, $LiMn_2O_4$ and $LiCoMnO_4$) of 10 wt.% in comparison with the physical mixture of $Li[Li_{0.2}Mn_{0.54}Ni_{0.13}Co_{0.13}]O_2$ and commercial $LiCoO_2$ in the same weight ratio at a current density of 250 mAh g⁻¹ (1C); (c) initial charge and discharge curves at a current density of 250 mAh g⁻¹ (1C) and (d) the first three CV profiles of $Li[Li_{0.2}Mn_{0.54}Ni_{0.13}Co_{0.13}]O_2$ nanoparticles modified with 10 wt.% $LiCoO_2$ shell at a scanning rate of 0.1 mV s⁻¹ “Bare LMNCO”: bare $Li[Li_{0.2}Mn_{0.54}Ni_{0.13}Co_{0.13}]O_2$ nanoparticles; “ $LM_xO_y-X@LMNCO$ ($M = Mn$ and Co), X is the weight content of shell materials”: $Li[Li_{0.2}Mn_{0.54}Ni_{0.13}Co_{0.13}]O_2$ nanoparticles modified with Li_xM_yO shell of X wt.%

from bare LMNCO. LMNCO coated by thicker 50 wt.% LiCoO₂ shell exhibits the highest discharge capacity of 188.2 mAh g⁻¹ but show poor capacity retention. The rapid capacity fading of LCO-50@LMNCO can be attributed to two possible reasons as follows: (1) the layered LiCoO₂ cathode suffers from structural instability when cycled at high voltage up to 4.8 V; (2) thicker shell composed of more LiCoO₂ nanoparticles can be more easily detached from LMNCO than thin shell during electrochemical cycling due to mechanical stress in repeated charge/discharge cycles. In contrast, LMNCO coated with LiCoO₂ shell in a low amount of 5 wt.% reveals both low specific capacity and poor capacity retention, probably because LiCoO₂ coverage on LMNCO particles is low due to the low amount of LiCoO₂. Fig. 5b compares cycling performances of LMNCO coated with different shell materials (LiCoO₂, LiMn₂O₄ and LiCoMnO₄) at 10 wt.% and simple mixture of LMNCO and 10 wt.% LiCoO₂. It can be seen that LMNCO coated with LiCoO₂ shell exhibits much better performance than LMNCO coated with LiMn₂O₄ and LiCoMnO₄. In addition, the LCO-10@LMNCO core–shell structure shows better performance than the physical mixture of LMNCO nanoparticles and LiCoO₂ nanoparticles in the same weight ratio, demonstrating the superiority of core–shell structure which have better structural comparability between LiCoO₂ shell and LMNCO core in the integrated “layered–layered” composite (Fig. 3d).

The electrochemical polarization of LMNCO cathode can be effectively reduced via coating ~10 nm LiCoO₂ shell on core LMNCO material, resulting in high reversibility of lithium ion insertion and extraction. As shown in Fig. 5c, the initial charge and discharge of LCO-10@LMNCO deliver high specific capacities of 295.8 mAh g⁻¹ and 187.5 mAh g⁻¹ at 1C, respectively, much higher than the initial charge capacity of 185.2 mAh g⁻¹ and discharge capacity of 114.5 mAh g⁻¹ from bare LMNCO. The overpotential between charge and discharge curves is also obviously decreased owing to the conductive LiCoO₂ shell on the core LMNCO nanoparticles. In comparison with CV profile of pristine LMNCO cathode in Fig. 4e, CV profiles of LCO-10@LMNCO in Fig. 5d demonstrate better reversibility of core–shell-structured composite. The first anodic peak at 4.11 V in the initial CV cycle is associated with oxidation of Ni²⁺/Ni⁴⁺ redox only from LMNCO cathode and Co³⁺/Co⁴⁺ redox from both LiCoO₂ shell and LMNCO core. The second peak at 4.67 V can be ascribed to electrochemical activation of Li₂MnO₃ region together with inevitable decomposition of electrolyte due to the high oxidation abilities of Mn⁴⁺, Ni⁴⁺ and Co⁴⁺ ions. Two corresponding cathodic peaks at 3.75 V and 3.17 V are related to combined reduction in Ni²⁺/Ni⁴⁺ and Co³⁺/Co⁴⁺ and reducing Mn⁴⁺ to Mn³⁺, respectively. The overpotential between main anodic and cathodic peaks related to oxidation and reduction in Ni²⁺/Ni⁴⁺ and Co³⁺/Co⁴⁺ is reduced to 0.37 V, smaller than 0.53 V from CV profile of bare LMNCO in Fig. 4e. After initial electrochemical activation, LCO-10@LMNCO shows significantly improved reversibility in subsequent CV cycles, resulting in high capacity and good capacity retention during high-rate cycling. However, the core–shell structure still shows a large irreversible capacity loss in the initial charge/discharge cycle corresponding to a low Coulombic efficiency of 63.5% (Fig. 5c), indicating LiCoO₂ shell cannot alleviate the initial capacity loss. Fabrication of the core–shell structure in this work can be generalized to other shell materials such as high-voltage spinel cathode material (e.g., LiMn_{1.5}Ni_{0.5}O₄) which can be used to reduce initial capacity loss of LMNCO cathode during the first electrochemical cycle. Employing high-voltage spinel cathode material as the shell can improve the structural stability of core–shell structure, because LiMn_{1.5}Ni_{0.5}O₄ is more stable than LiCoO₂ and LMNCO under the high voltage up to 4.8 V [57]. Another alternative approach is to prepare LiM_xO_y (M = Mn, Co and Ni) shell via ALD from Li₂O and M_xO_y, followed by heat treatment. The LiM_xO_y ALD shells can be chemically bonded to the surface of

LMNCO particles via oxygen bonds, and thus can restrict the oxygen evolution and structural rearrangement of LMNCO cathode in the initial cycle [46].

3.3. Hierarchical functional layers coated on Li[Li_{0.2}Mn_{0.54}Ni_{0.13}Co_{0.13}]O₂ nanoparticles for maximized performance

In order to reduce the initial capacity loss and improve cycleability and rate capability at high charge/discharge rates all together, we combine the ALD coating with the core–shell structure. As discussed above, 6ZrO₂ ALD layers can effectively restrict electrolyte composition and stabilize the rearranged layered structure after initial activation of LMNCO, and thus improve initial Coulombic efficiency and cycleability of LMNCO. On the other hand, 10 wt.% LiCoO₂ shell can increase capacities of LMNCO at high charge/discharge rates, due to enhanced electronic conductivity from LiCoO₂. Hence, we combine ALD and core–shell structure and fabricate hierarchical functional layers on LMNCO by depositing 10 wt.% LiCoO₂ (~10 nm thick) on LMNCO first followed by deposition of 6ZrO₂ ALD layers (~1 nm thick) (marked as 6ZrO₂ ALD@LCO-10@LMNCO).

Fig. 6a compares cycling performances of ALD-coated core–shell structure, core–shell structure, ALD-coated LMNCO, and bare LMNCO. Corresponding results are also summarized in Table 1. Obviously, 6ZrO₂ ALD@LCO-10@LMNCO delivers the highest initial discharge capacity of 259.8 mAh g⁻¹ at 1C, significantly higher than 187.5 mAh g⁻¹ of LCO-10@LMNCO, 152.9 mAh g⁻¹ of 6ZrO₂ ALD@LMNCO and 114.5 mAh g⁻¹ of bare LMNCO. This result is also better than the capacity of LMNCO coated with double shells (2 wt.% AlPO₄ + 3 wt.% Al₂O₃ or 2 wt.% CoPO₄ + 3 wt.% Al₂O₃) [29] and other surface-modified LMNCO cathodes reported in literature [24,31]. It is also noted that ALD-coated core–shell structure delivers a final capacity of 184.0 mAh g⁻¹ after 100 electrochemical cycles, which is three times that from bare LMNCO (65.9 mAh g⁻¹). The remarkably increased capacity and enhanced cycleability of 6ZrO₂ ALD@LCO-10@LMNCO can be attributed to combined effects from LiCoO₂ shell and ZrO₂ coating in improving performance of LMNCO. Fig. 6b and c reveals the superior rate capability of this nanoarchitected composite cathode modified with nano-sized LiCoO₂ shell (~10 nm) and sub-nano-sized ZrO₂ coating (~1 nm). As shown in Fig. 6b, 6ZrO₂ ALD@LCO-10@LMNCO shows initial discharge capacities of 296.4, 259.8, 156.6 and 104.2 mAh g⁻¹ at 0.1C, 1C, 5C and 10C, which are higher than capacities of LMNCO based cathodes reported previously, such as graphene-enwrapped LMNCO hybrid cathode [24,36], LMNCO coated with oxides [12,25,33], persulfate treated LMNCO [30] and LMNCO coated with double shells [29]. Fig. 6c compares rate performances of 6ZrO₂ ALD@LCO-10@LMNCO and bare LMNCO, which clearly shows significantly enhanced rate capability, cycleability and reversibility of LMNCO coated with hierarchical functional layers.

The improved electrochemical property of 6ZrO₂ ALD@LCO-10@LMNCO can be understood from its CV curves in Fig. 6d. After initial activation of 6ZrO₂ ALD@LCO-10@LMNCO in the first CV cycle, the overpotential of the predominant pair of anodic/cathodic peaks is 0.17 V in subsequent second and third CV cycles, which is much smaller than 0.28 V from LCO-10@LMNCO (Fig. 5d), 0.30 V from 6ZrO₂ ALD@LMNCO (Fig. 4e) and 0.43 V from bare LMNCO (Fig. 4f), indicating better reversibility of Ni²⁺/Ni⁴⁺ and Co³⁺/Co⁴⁺ redox in 6ZrO₂ ALD@LCO-10@LMNCO. The second cathodic peak related to reduction in Mn³⁺/Mn⁴⁺ is very sharp and shifts to the higher voltage at 3.25 V, suggesting the enhanced contribution of active MnO₂ component in lithiation and delithiation after initial activation of 6ZrO₂ ALD@LCO-10@LMNCO in the first cycle. Better reversibility of transition metal redox pairs can be mainly attributed to the improved electronic conductivity from LiCoO₂ shell. A

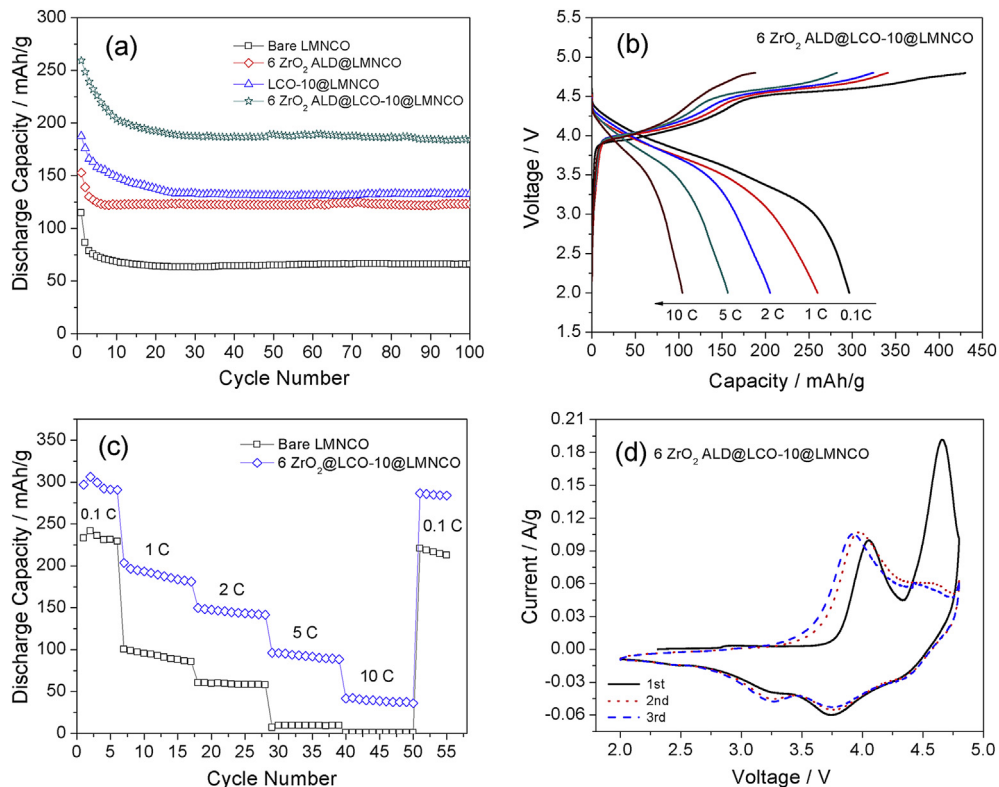


Fig. 6. Electrochemical performances of $\text{Li}[\text{Li}_{0.2}\text{Mn}_{0.54}\text{Ni}_{0.13}\text{Co}_{0.13}] \text{O}_2$ nanoparticles modified with 10 wt.% LiCoO_2 shell followed by coating with 6 ZrO_2 ALD layers cycled in a voltage range of 2.0–4.8 V: (a) cycling performances at a current density of 250 mAh g^{-1} (1C) in comparison with bare and $\text{Li}[\text{Li}_{0.2}\text{Mn}_{0.54}\text{Ni}_{0.13}\text{Co}_{0.13}] \text{O}_2$ nanoparticles coated 10 wt.% LiCoO_2 shell (LCO-10@LMNCO) or 6 ZrO_2 ALD layers (6 ZrO_2 ALD@LMNCO); (b) initial charge and discharge curves and (c) rate performance at a series of current densities; and (d) the first three CV profiles at a scanning rate of 0.1 mV s^{-1} . “Bare LMNCO”: bare $\text{Li}[\text{Li}_{0.2}\text{Mn}_{0.54}\text{Ni}_{0.13}\text{Co}_{0.13}] \text{O}_2$ nanoparticles; “6 ZrO_2 ALD@LCO-10@LMNCO”: $\text{Li}[\text{Li}_{0.2}\text{Mn}_{0.54}\text{Ni}_{0.13}\text{Co}_{0.13}] \text{O}_2$ nanoparticles modified with LiCoO_2 shell of 10 wt.%, followed by being coated with 6 ZrO_2 ALD layers.

weak anodic/cathodic peak pair appears around ~4.5 V, different from CV profiles of LCO-10@LMNCO (Fig. 5d), 6 ZrO_2 ALD@LMNCO (Fig. 4e) and bare LMNCO (Fig. 4f). Such extra anodic and cathodic peaks at ~4.5 V may be due to a cumulative effect from hierarchical functional coatings to preserve oxygen ion vacancies for reversible insertion and extraction of lithium ions after electrochemical activation of Li_2MnO_3 region. Overall, CV measurement reveals that ZrO_2 ALD coating on core–shell-structured LCO-10@LMNCO can effectively inhibit the rearrangement of metal ions and thus restrict structural degradation of core LMNCO cathode, resulting in high

reversibility, cycleability and rate capability of Li-excess layered cathode material.

4. Conclusions

Surface modifications on $\text{Li}[\text{Li}_{0.2}\text{Mn}_{0.54}\text{Ni}_{0.13}\text{Co}_{0.13}] \text{O}_2$ nanoparticles have been demonstrated to improve electrochemical performance of Li-excess layered cathode materials. Ultrathin and conformal ALD oxide coatings can effectively restrict decomposition of electrolyte and stabilize the layered structure of LMNCO, and thus reduce initial capacity loss and enhance cycleability of LMNCO. ZrO_2 is the most effective oxide coating for improved electrochemical performance of LMNCO electrodes, followed by ZnO and Al_2O_3 . The optimal thickness of ZrO_2 coating for LMNCO is ~1 nm via 6ALD growth layers. LMNCO nanoparticles coated with 6 ZrO_2 ALD layers delivers an initial discharge capacity of 274.9 mAh g^{-1} at 0.1C with a high Coulombic efficiency of 83.3%, while bare LMNCO shows a lower initial discharge capacity of 228.4 mAh g^{-1} and Coulombic efficiency of only 58.3%. In addition, rate capability of LMNCO can be improved by fabricating core–shell structure with LMNCO as core and Li-stoichiometric active material (LiCoO_2 , LiMn_2O_4 , and LiCoMnO_4) as shell and LiCoO_2 shell is found to have the best effect. The optimal weight content of LiCoO_2 shell is 10 wt.% for maximized performance of core–shell electrode, yielding a ~10 nm thick LiCoO_2 shell delicately integrated on the surface of LMNCO particles. LCO-10@LMNCO shows the initial discharge capacity of 187.5 mAh g^{-1} at 1C and retains 132.8 mAh g^{-1} after 100 electrochemical cycles, which are much higher than the initial discharge capacity of 114.5 mAh g^{-1} and final capacity of 65.9 mAh g^{-1} from bare LMNCO, due to enhanced electronic conductivity from LiCoO_2 .

Table 1

Initial discharge capacity and final capacity after 100 electrochemical cycles delivered by $\text{Li}[\text{Li}_{0.2}\text{Mn}_{0.54}\text{Ni}_{0.13}\text{Co}_{0.13}] \text{O}_2$ nanoparticles modified with 10 wt.% LiCoO_2 shell followed by coating with 6 ZrO_2 ALD layers in comparison with bare cathode and different surface modified cathodes.

Electrodes cycled at 1C	Initial discharge capacity/ mAh g^{-1}	100th discharge capacity/ mAh g^{-1}	Reference
6 ZrO_2 ALD@LCO-10@LMNCO	259.8	184.0	This work
LCO-10@LMNCO	187.5	132.8	This work
6 ZrO_2 ALD@LMNCO	152.9	123.0	This work
Bare LMNCO	114.5	65.9	This work
LMNCO coated with 2 wt.% AlPO_4 + 3 wt.% Al_2O_3	~230	N/A	Ref. [29]
LMNCO coated with 2 wt.% CoPO_4 + 3 wt.% Al_2O_3	~225	N/A	Ref. [29]
LMNCO treated with 50 wt.% $\text{Na}_2\text{S}_2\text{O}_8$	194.8	173.3 at 50th cycle	Ref. [30]
LMNCO enwrapped with 4.9 wt.% graphene at 0.5C	~200	~165	Ref. [24]

and reduced electrochemical polarization of core–shell structure during cycling. Finally, ALD is combined with core–shell structure and hierarchical functional layers are fabricated on LMNCO by depositing 10 wt.% LiCoO₂ (~10 nm thick) on LMNCO first followed by deposition of 6ZrO₂ ALD layers (~1 nm thick). Such nano-architected cathode exhibits a very high initial discharge capacity of 259.8 mAh g⁻¹ at 1C and retains a final capacity of 184.0 mAh g⁻¹ after 100 electrochemical cycles which is three times that from bare LMNCO (65.9 mAh g⁻¹). Such results are also higher than capacities of other surface modified LMNCO reported in literature. It is also noted that surface modification via hierarchical functional layers can be applied to other cathode materials or anode materials for advanced lithium ion batteries.

Acknowledgments

This work is supported by LABOR-RCS grant. The authors also acknowledge Materials Characterization Center (MCC) at LSU for using XRD, SEM and TEM.

References

- [1] J.B. Goodenough, K.S. Park, *J. Am. Chem. Soc.* 135 (2013) 1167–1176.
- [2] R. Mukherjee, R. Krishnan, T.M. Lu, N. Koratkar, *Nano Energy* 1 (2012) 518–533.
- [3] L. Hu, N. Liu, M. Eskilsson, G. Zheng, J. McDonough, L. Wågberg, Y. Cui, *Nano Energy* 2 (2013) 138–145.
- [4] I. Meschini, F. Nobili, M. Mancini, R. Marassi, R. Tossici, A. Savoini, M.L. Focarete, F. Croce, *J. Power Sources* 226 (2013) 241–248.
- [5] P. He, H. Yu, D. Li, H. Zhou, *J. Mater. Chem.* 22 (2012) 3680–3695.
- [6] A.R. Armstrong, M. Holzapfel, P. Novák, C.S. Johnson, S.H. Kang, M.M. Thackeray, P.G. Bruce, *J. Am. Chem. Soc.* 128 (2006) 8694–8698.
- [7] T.A. Arunkumar, Y. Wu, A. Manthiram, *Chem. Mater.* 19 (2007) 3067–3073.
- [8] T.A. Arunkumar, E. Alvarez, A. Manthiram, *J. Electrochem. Soc.* 154 (2007) A770–A775.
- [9] Y. Wu, A. Manthiram, *J. Power Sources* 183 (2008) 749–754.
- [10] K.A. Jarvis, Z. Deng, L.F. Allard, A. Manthiram, P.J. Ferreira, *Chem. Mater.* 23 (2011) 3614–3621.
- [11] E.S. Lee, A. Huq, H.Y. Chang, A. Manthiram, *Chem. Mater.* 24 (2012) 600–612.
- [12] W. He, J. Qian, Y. Cao, X. Ai, H. Yang, *RSC Adv.* 2 (2012) 3423–3429.
- [13] S.H. Yu, T. Yoon, J. Mun, S. Park, Y.S. Kang, J.H. Park, S.M. Oh, Y.E. Sung, *J. Mater. Chem. A* 1 (2013) 2833–2839.
- [14] D. Kim, G. Sandi, J.R. Croy, K.G. Gallagher, S.H. Kang, E. Lee, M.D. Slater, C.S. Johnson, M.M. Thackeray, *J. Electrochem. Soc.* 160 (2013) A31–A38.
- [15] Y. Wang, X. Bie, K. Nikolowski, H. Ehrenberg, F. Du, M. Hinterstein, C. Wang, G. Chen, Y. Wei, *J. Phys. Chem. C* 117 (2013) 3279–3286.
- [16] B. Xu, C.R. Fell, M. Chi, Y.S. Meng, *Energy Environ. Sci.* 4 (2011) 2223–2233.
- [17] N. Yabuuchi, K. Yoshii, S.T. Myung, I. Nakai, S. Komaba, *J. Am. Chem. Soc.* 133 (2011) 4404–4419.
- [18] M. Jiang, B. Key, Y.S. Meng, C.P. Grey, *Chem. Mater.* 21 (2009) 2733–2745.
- [19] J. Hong, H.D. Lim, M. Lee, S.W. Kim, H. Kim, S.T. Oh, G.C. Chung, K. Kang, *Chem. Mater.* 24 (2012) 2692–2697.
- [20] M. Gu, I. Belharouak, J. Zheng, H. Wu, J. Xiao, A. Genc, K. Amine, S. Thevuthasan, D.R. Baer, J.G. Zhang, N.D. Browning, J. Liu, C. Wang, *ACS Nano* 7 (2013) 760–767.
- [21] D. Wang, I. Belharouak, G. Zhou, K. Amine, *Adv. Funct. Mater.* 23 (2013) 1070–1075.
- [22] A. Boulineau, L. Simonin, J.F. Colin, E. Canevet, L. Daniel, S. Patoux, *Chem. Mater.* 24 (2012) 3558–3566.
- [23] F. Amalraj, M. Talianker, B. Markovsky, D. Sharon, L. Burlaka, G. Shafir, E. Zinigrad, O. Haik, D. Aurbach, J. Lampert, M. Schulz-Dobrick, A. Garsuch, *J. Electrochem. Soc.* 160 (2013) A324–A337.
- [24] K.C. Jiang, X.L. Wu, Y.X. Yin, J.S. Lee, J. Kim, Y.G. Guo, *ACS Appl. Mater. Interfaces* 4 (2012) 4858–4863.
- [25] Y.S. Jung, A.S. Cavanagh, Y. Yan, S.M. George, A. Manthiram, *J. Electrochem. Soc.* 158 (2011) A1298–A1302.
- [26] Y. Wu, A. Manthiram, *Solid State Ionics* 180 (2009) 50–56.
- [27] G.R. Li, X. Feng, Y. Ding, S.H. Ye, X.P. Gao, *Electrochim. Acta* 78 (2012) 308–315.
- [28] Y. Liu, S. Liu, Y. Wang, L. Chen, X. Chen, *J. Power Sources* 222 (2013) 455–460.
- [29] Q.Y. Wang, J. Liu, A. Vadivel Murugan, A. Manthiram, *J. Mater. Chem.* 19 (2009) 4965–4972.
- [30] J. Zheng, S. Deng, Z. Shi, H. Xu, H. Xu, Y. Deng, Z. Zhang, G. Chen, *J. Power Sources* 221 (2013) 108–113.
- [31] T. Zhao, S. Chen, L. Li, X. Zhang, R. Chen, I. Belharouak, F. Wu, K. Amine, *J. Power Sources* 228 (2013) 206–213.
- [32] H. Yim, W.Y. Kong, Y.C. Kim, S.J. Yoon, J.W. Choi, *J. Solid State Chem.* 196 (2012) 288–292.
- [33] S.J. Shi, J.P. Tu, Y.Y. Tang, X.Y. Liu, Y.Q. Zhang, X.L. Wang, C.D. Gu, *Electrochim. Acta* 88 (2013) 671–679.
- [34] J. Wang, B. Qiu, H. Cao, Y. Xia, Z. Liu, *J. Power Sources* 218 (2012) 128–133.
- [35] S.K. Martha, J. Nanda, G.M. Veith, N.J. Dudney, *J. Power Sources* 199 (2012) 220–226.
- [36] Z. He, Z. Wang, H. Guo, X. Li, X. Wu, P. Yue, J. Wang, *Mater. Lett.* 91 (2013) 261–264.
- [37] Z. Chen, Y. Qin, K. Amine, Y.K. Sun, *J. Mater. Chem.* 20 (2010) 7606–7612.
- [38] J. Zhao, Y. Wang, *J. Phys. Chem. C* 116 (2012) 11867–11876.
- [39] J. Zhao, Y. Wang, *J. Solid State Electrochem.* 17 (2013) 1049–1058.
- [40] J. Lu, Q. Peng, W. Wang, C. Nan, L. Li, Y. Li, *J. Am. Chem. Soc.* 135 (2013) 1649–1652.
- [41] Y.S. Jung, A.S. Cavanagh, L.A. Riley, S.H. Kang, A.C. Dillon, M.D. Groner, S.M. George, S.H. Lee, *Adv. Mater.* 22 (2010) 2172–2176.
- [42] I.D. Scott, Y.S. Jung, A.S. Cavanagh, Y. Yan, A.C. Dillon, S.M. George, S.H. Lee, *Nano Lett.* 11 (2011) 414–418.
- [43] X. Meng, X.Q. Yang, X. Sun, *Adv. Mater.* 24 (2012) 3589–3615.
- [44] S. Boukalfa, K. Evanoff, G. Yushin, *Energy Environ. Sci.* 5 (2012) 6872–6879.
- [45] H. Lee, J.K. Hwang, J.W. Nam, S.U. Lee, J.T. Kim, S.M. Koo, A. Baunemann, R.A. Fischer, M.M. Sung, *Angew. Chem. Int. Ed.* 48 (2009) 4536–4539.
- [46] J. Zhao, Y. Wang, G. Qu, J.C. Flake, *Chem. Commun.* 48 (2012) 8108–8110.
- [47] Y.K. Sun, Z. Chen, H.J. Noh, D.J. Lee, H.G. Jung, Y. Ren, S. Wang, C.S. Yoon, S.T. Myung, K. Amine, *Nat. Mater.* 11 (2012) 942–947.
- [48] Y. Cho, S. Lee, Y. Lee, T. Hong, J. Cho, *Adv. Energy Mater.* 1 (2011) 821–828.
- [49] S.T. Myung, K.S. Lee, D.W. Kim, B. Scrosati, Y.K. Sun, *Energy Environ. Sci.* 4 (2011) 935–939.
- [50] Y.K. Sun, D.H. Kim, C.S. Yoon, S.T. Myung, J. Prakash, K. Amine, *Adv. Funct. Mater.* 20 (2010) 485–491.
- [51] X. Yang, X. Wang, Q. Wei, H. Shu, L. Liu, S. Yang, B. Hu, Y. Song, G. Zou, L. Hu, L. Yi, *J. Mater. Chem.* 22 (2012) 19666–19672.
- [52] Q.Q. Qiao, H.Z. Zhang, G.R. Li, S.H. Ye, C.W. Wang, X.P. Gao, *J. Mater. Chem. A* 1 (2013) 5262–5268.
- [53] F. Amalraj, D. Kovacheva, M. Talianker, L. Zeiri, J. Grinblat, N. Leifer, G. Goobes, B. Markovsky, D. Aurbach, *J. Electrochem. Soc.* 157 (2010) A1121–A1130.
- [54] Y. Wu, A. Manthiram, *Electrochem. Solid-State Lett.* 9 (2006) A221–A224.
- [55] T.H. Cho, Y. Shiosaki, H. Noguchi, *J. Power Sources* 159 (2006) 1322–1327.
- [56] M. Park, X. Zhang, M. Chung, G.B. Less, A.M. Sastry, *J. Power Sources* 195 (2010) 7904–7929.
- [57] X. Zhang, F. Cheng, J. Yang, J. Chen, *Nano Lett.* 13 (2013) 2822–2825.